# High Precision Control of Flux Switching Linear Rotary Machine for Reelwinder

Kaikai Guo
*School of Electrical and Information Engineering*
*Anhui University of Science and Technology*
Huainan, China
guokai0072000@gmail.com

Youguang Guo
*School of Electrical and Data Engineering*
*University of Technology Sydney*
Sydney, NSW
Youguang.guo-1@uts.edu.au

***Abstract*—Since there is still large amplitude of the detent force of a flux switching linear rotary machine, the response time is long using space vector pulse width modulation control method when it works in linear motion at low speed. In order to reduce the disturbances, the sliding mode control method is adopted both in linear and rotary motions direction. An improved two degree of freedom permanent magnet flux linkage sliding mode observer is designed, which can suppress the torque and thrust pulsation of the motor and retain the torque and thrust output capacity. The stability and accuracy of the system have been greatly improved, which are verified by the experiment test.**

***Keywords—flux switching linear rotary machine, high precision, sliding mode observer***

## I. Introduction

The decoupling control of linear rotating motor is one of the hot research issues. The helical motion of a 2-degree-of-freedom (2-DOF) linear rotary induction motor was achieved, and its torque and force were studied, which can influence each other [1]. The voltage, current, or flux linkage of multiphase magnetically levitated rotary-linear machine was defined by the two frames related with the rotary and linear motions [2]. The decoupling control of flux reversal linear rotary machine (LRM) was achieved based on ideal linear mathematical model, but the response time is long when the machine is at low speed [3]. A fault tolerant control method of permanent magnet (PM) linear vernier motor with an open winding was presented to ensure its continued operation [4]. In order to improve the robustness and the current bandwidth of the PM linear synchronous motor (PMLSM), a high-performance current regulation scheme was introduced in [5]. The control of a PMLSM was achieved by an improved sliding-mode control (SMC) strategy [6]. An improved control strategy of PMSM was proposed by building a linear quadratic regulator, which can consider the speed and thrust [7]. Based on the heave-motion mechanism of buoy, a high-speed operation damping control strategy of PM linear generator was proposed by a wave energy converter [8]. A model predictive control model of an flux-switching (FS) PM linear machine was developed and implemented to reduce the thrust ripple by building a improved voltage vectors model [9]. The mover position of a PM linear motor (PMLM) was detected by a contactless magnetic sensor [10]. The topologies, advanced modeling, design and control of linear motors were presented with case studies related to industrial applications [11]. An improved SMC model of PMLM was designed and an equivalent fast terminal SMC law was concluded [12]. The resonant 2-DOF proportional integral (PI) derivative controller was investigated, which can suppress the harmonics of the current component combined with the traditional PI controller [13]. An iterative estimation algorithm of a surface PMLSM was conducted to reduce the effect of the detent force on the estimation of the initial mover position [14]. An active disturbance rejection control algorithm was used to suppress the disturbances of the control system by building a reduced-order extended state observer [15]. An periodical adaptive disturbance observer of PMLSMs was presented in [16]. An on-line simultaneous computation method was proposed to measure the model parameters and position of a PMLSM by the measurement model with Fourier series [17]. In order to reduce the flux and thrust ripples, an improved direct thrust control of PMLSM was achieved by the duty ratio control strategy, which can select the voltage vector from the switching table and take the mover speed into consideration [18].

In order to shorten the response time of FS-LRM, a high precision control system is established for reelwinder application, which can achieve high control accuracy and response speed. According to the winding characteristic, the winding arrangements, back electromotive force (EMF) and flux linkage are analyzed. The mathematical model of the motor is established by dual-*dq* mover coordinate system, then the 2-DOF sliding mode observer is built and the simulation is conducted.

## II. Control Characteristic Analysis

### A. Winding Characteristic Analysis

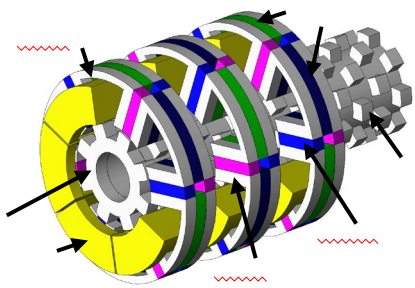

Fig. 1. The topology of FS-LRM

Fig. 1 reveals the topology of FS-LRM, and the optimization design and structure feature are introduced in [19][20]. Fig. 2 shows the cogging torque and detent force waveforms when the mover is at different axial and circumferential positions, respectively. It is noticed that the changing trend of cogging torque or detent force remains the same, and the amplitude of the detent force is large, which is the main cause of unstable operation of the motor at low-

This work was supported by the National Natural Science Foundation under Grant 51905003, Natural Science Foundation of Anhui Province under Grant 1908085QE207, China Postdoctoral Science Foundation under Grant 2019M652161, and Talent Introduction Foundation of AUST under Grant 12365.

speed condition, and it can be suppressed by the harmonic injection method.

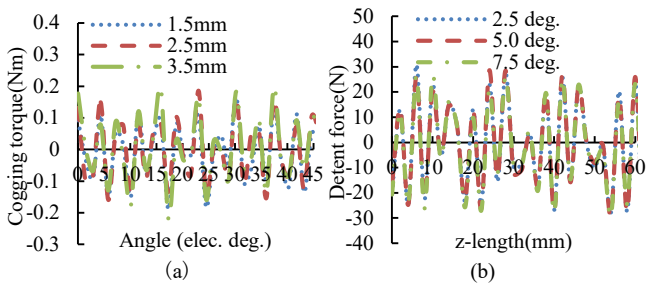


Fig. 2. Cogging torque and detent force waveforms, (a) cogging torque, and (b) detent force.

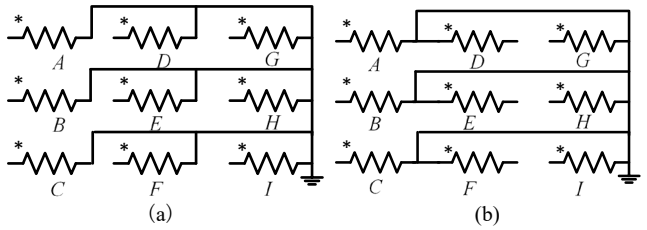


Fig. 3. Winding arrangements with common midpoint, (a) rotary motion, and (b) linear motion.

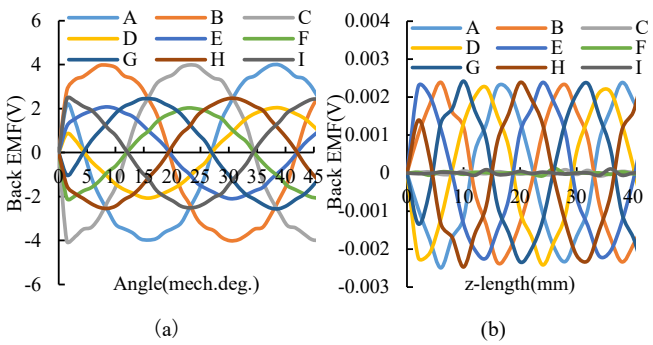


Fig. 4. Back EMF waveforms, (a) rotary motion, and (b) linear motion.

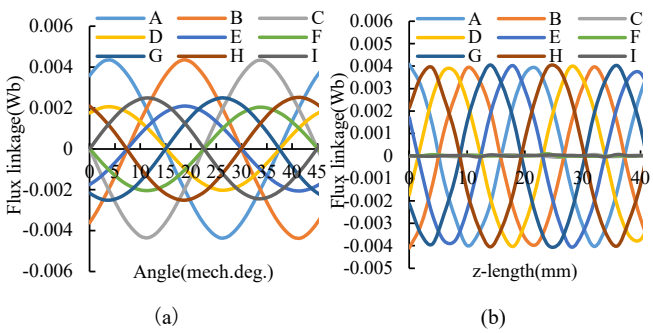


Fig. 5. Flux linkage waveforms, (a) rotary motion, and (b) linear motion.

Fig. 3 reveals the winding arrangements. The windings with common midpoint are adopted, and the input and output terminals of windings (*D*, *E*, *F*) are different when the motor works in different motion directions. Namely, the linking method of the midpoint is changed. Figs. 4 and 5 show respectively the back EMF and flux linkage waveforms of rotary and linear motions when the mover placed at the initial position. The rotary and linear velocities are 1200 r/min and 0.004 m/s, respectively. At the initial position, the flux linkages of windings (*C*, *F*, *I*) are equal to zero and the other windings (*A*, *D*, *G*) and (*B*, *E*, *H*) would generate the stator magnetic flux when it is in linear motion. The nine phase windings can generate the stator magnetic flux when it works in rotary motion.

### *B. Mathematical Model under Mover Coordinate System*

The dual-*dq* coordinate system is adopted, and then the voltage equation under the mover coordinate system is

$$\begin{cases} u_{dd} = L\dfrac{di_{dd}}{dt} - \omega L i_{dq} - \dfrac{2\pi}{\tau_z} v_z L i_{qq} + R_{dd} i_{dd} \\ u_{dq} = L\dfrac{di_{dq}}{dt} + \omega(L i_{dd} + \psi_{pm}) - \dfrac{2\pi}{\tau_z} v_z L i_{qq} + R_{dq} i_{dq} \\ u_{qd} = L\dfrac{di_{qd}}{dt} - \omega L i_{qq} + \dfrac{2\pi}{\tau_z} v_z (L i_{dd} + \psi_{pm}) + R_{qd} i_{qd} \\ u_{qq} = L\dfrac{di_{qq}}{dt} + \omega L i_{qd} + \dfrac{2\pi}{\tau_z} v_z L i_{dq} + R_{qq} i_{qq} \end{cases} \tag{1}$$

where $L$ is the winding inductance of single phase. $\omega$ is the electrical angular velocity of the mover in circumferential direction. $\tau_z$ and $v_z$ are the pole pitch and linear velocity in axial direction, respectively.

When $i_{dd}$=$i_{qq}$=0, the torque and force expressions are

$$\begin{aligned} T_e &= -i_{dq}\psi_{dd} + i_{qd}\psi_{qq} \\ &= -i_{dq}(L_{dd} i_{dd} + \psi_{PMdd}) + i_{qd}(L_{qq} i_{qq} + \psi_{PMqq}) = -\frac{9}{4} i_{dq}\psi_{PM\max} \end{aligned} \tag{2}$$

$$\begin{aligned} F_e &= 2\pi(-i_{qd}\psi_{dd} + i_{dq}\psi_{qq})/\tau \\ &= -2\pi i_{qd}(L_{dd} i_{dd} + \psi_{PMdd})/\tau + 2\pi i_{dq}(L_{qq} i_{qq} + \psi_{PMqq})/\tau \\ &= -9\pi i_{qd}\psi_{PM\max}/2\tau \end{aligned} \tag{3}$$

where, $i_{dq}$ and $i_{qd}$ are the *dq* axis current component and is the *qd* axis current component, respectively.

## III. Control Strategy Analysis

Since the inductances of *dd*-axis, *qq*-axis, *dq*-axis and *qd*-axis in FS-LRM are very close, the reluctance torque and thrust are very small. Then the $i_{dd}$=$i_{qq}$=0 control method is adopted in the constant torque region.

### *A. $i_{dd}$=$i_{qq}$=0 Control Strategy*

According to (1), the dual-*dq* axis voltages are decoupled each other, and the approximate decoupling is achieved by the current PI regulator to get the reference voltage value. $\omega L i_{dq}$ and $\omega(L i_{dd}+\psi_{pm})$, $\omega L i_{qd}$ and $2\pi v_z(L i_{dd}+\psi_{pm})/\tau_z$ are taken as disturbance term of rotary and linear motions to actualize feedforward compensation and eliminate the voltage coupling of *dq* axis and *qd* axis, respectively.

$u_{dd}^*$, $u_{dq}^*$, $u_{qd}^*$ and $u_{qq}^*$ are the current bias sum of the output term of the current PI regulator and the feed forward decoupling term. Then the expression is

$$\begin{cases} u_{dd}^{*} = \left(K_a + \dfrac{K_b}{s}\right)\left(i_{dd}^{*} - i_{dd}\right) + \Delta u_{dd} \\ u_{qq}^{*} = \left(K_a + \dfrac{K_b}{s}\right)\left(i_{qq}^{*} - i_{qq}\right) + \Delta u_{qq} \\ u_{dq}^{*} = \left(K_a + \dfrac{K_b}{s}\right)\left(i_{dq}^{*} - i_{dq}\right) + \Delta u_{dq} \\ u_{qd}^{*} = \left(K_a + \dfrac{K_b}{s}\right)\left(i_{qd}^{*} - i_{qd}\right) + \Delta u_{qd} \end{cases} \tag{4}$$

where $K_a$ and $K_b$ are the proportional coefficient and integral coefficient of the current PI regulator, respectively. $\Delta u_{dd}$, $\Delta u_{qq}$, $\Delta u_{dq}$ and $\Delta u_{qd}$ are the decoupling components of *dd*-axis, *qq*-axis, *dq*-axis and *qd*-axis, respectively.

### *B. Parameter Identification of PM Flux Linkage*

Since the PM flux linkage is variable when the mover is at different positions, the accuracy of flux linkage can not be guaranteed by the relation of the current and flux linkage. The traditional control method such as the extended Kalman filter method involves matrix operation, and the nonlinear adaptive element method needs to select a proper convergence factor, otherwise the observer may not converge. Then the 2-DOF PM flux linkage sliding mode observer is designed, which can be used to identify the PM flux linkage under different mover positions.

Since the direct current component is convenient for the design of the filter, which can reduce chattering and observation error. When the saturation and loss of the motor are ignored, the expressions of the state equation in dual-*dq* coordinate system are

$$\begin{cases} \dfrac{di_{dd}}{dt} = \dfrac{u_{dd} - R_{dd} i_{dd}}{L} + \omega i_{dq} + \dfrac{2\pi}{\tau_z} v_z i_{qd} \\ \dfrac{di_{dq}}{dt} = \dfrac{u_{dq} - \omega \psi_{pm} - R_{dq} i_{dq}}{L} - \omega i_{dd} + \dfrac{2\pi}{\tau_z} v_z i_{qq} \\ \dfrac{di_{qd}}{dt} = \dfrac{u_{qd} - \dfrac{2\pi}{\tau_z} v_z \psi_{pm} - R_{qd} i_{qd}}{L} + \omega i_{qq} - \dfrac{2\pi}{\tau_z} v_z i_{dd} \\ \dfrac{di_{qq}}{dt} = \dfrac{u_{qq} - R_{qq} i_{qq}}{L} - \omega i_{qd} - \dfrac{2\pi}{\tau_z} v_z i_{dq} \end{cases} \tag{5}$$

Since the PM flux linkage exists only in the *dq*-axis and *qd*-axis, the *dq*-axis and *qd*-axis equations are

$$\begin{cases} \dfrac{di_{dq}}{dt} = A i_{dq} + B u_{dq} + K_{dq} e_{dq} \\ \dfrac{di_{qd}}{dt} = A i_{qd} + B u_{qd} + K_{qd} e_{qd} \end{cases} \tag{6}$$

where $A_{dq}$=-$R_{dq}/L$, $A_{qd}$=-$R_{qd}/L$,$B$=1/$L$, $K_{dq}$= $K_{qd}$ =-$B$, $e_{dq}$, $e_{qd}$ are the back EMF of PM flux linkage in *dq*-axis and *qd*-axis, respectively.

Then the sliding mode observer equations are constructed as

$$\begin{cases} \dfrac{d\hat{i}_{dq}}{dt} = A_{dq} \hat{i}_{dq} + B u_{dq} - \dfrac{K_{odq}}{L} \operatorname{sgn}(\hat{i}_{dq} - i_{dq}) \\ \dfrac{d\hat{i}_{qd}}{dt} = A_{qd} \hat{i}_{qd} + B u_{qd} - \dfrac{K_{oqd}}{L} \operatorname{sgn}(\hat{i}_{qd} - i_{qd}) \end{cases} \tag{7}$$

where "^"is the estimated value, $K_{dq}$, $K_{qd}$ are the switching gains of the observer.

$$\operatorname{sgn}\left(\hat{i}_s - i_s\right) = \begin{cases} 1 & \hat{i}_s - i_s > 0 \\ -1 & \hat{i}_s - i_s < 0 \end{cases} \tag{8}$$

where $i_s$=$i_{dq}$ or $i_{qd}$.

The error dynamic equation of sliding mode observer is

$$\begin{cases} \dfrac{d\tilde{i}_{dq}}{dt} = A_{dq} \tilde{i}_{dq} - K_{dq} e_{dq} - \dfrac{K_{odq}}{L} \operatorname{sgn}(\hat{i}_{dq} - i_{dq}) \\ \dfrac{d\tilde{i}_{qd}}{dt} = A_{qd} \tilde{i}_{qd} - K_{qd} e_{qd} - \dfrac{K_{oqd}}{L} \operatorname{sgn}(\hat{i}_{qd} - i_{qd}) \end{cases} \tag{9}$$

where $\tilde{i}_{dq} = \hat{i}_{dq} - i_{dq}$, $\tilde{i}_{qd} = \hat{i}_{qd} - i_{qd}$ are the observational error. $\tilde{i}_{dq} = 0$ , $\tilde{i}_{qd} = 0$ can be taken as the slipform hyperplane. The dynamic performance of the error depends on the PM rotary back EMF.

If $\tilde{i}_{dq}^{\mathrm{T}} \tilde{i}_{dq} \le 0$ , $\tilde{i}_{qd}^{\mathrm{T}} \tilde{i}_{qd} \le 0$ , the error dynamic equation is asymptotically stable. Then

$$\begin{cases} \tilde{i}_{dq} \dfrac{\mathrm{d}\tilde{i}_{dq}}{\mathrm{d}t} = -A_{dq} \tilde{i}_{dq}^{2} - K_{dq} e_{dq} \tilde{i}_{dq} - \dfrac{K_{odq}}{L} \tilde{i}_{dq} \operatorname{sgn}(\hat{i}_{dq} - i_{dq}) \\ \tilde{i}_{qd} \dfrac{\mathrm{d}\tilde{i}_{qd}}{\mathrm{d}t} = -A_{qd} \tilde{i}_{qd}^{2} - K_{qd} e_{qd} \tilde{i}_{qd} - \dfrac{K_{oqd}}{L} \tilde{i}_{qd} \operatorname{sgn}(\hat{i}_{qd} - i_{qd}) \end{cases} \tag{10}$$

When $K_{odq}$>$e_{dq}$, $K_{oqd}$>$e_{qd}$, the error dynamic equation is asymptotically stable and the observation equation is convergent.

In order to suppress chattering adequately, the following adaptive law can be adopted

$$\begin{cases} K_{odq} = \lambda_{dq} \hat{e}_{dq}, \lambda_{dq} > 1 \\ K_{oqd} = \lambda_{qd} \hat{e}_{qd}, \lambda_{qd} > 1 \end{cases} \tag{11}$$

When the state point reaches the hyperplane,

$$\begin{cases} \tilde{i}_{dq} = \dfrac{\mathrm{d}\tilde{i}_{dq}}{\mathrm{d}t} = 0 \\ \tilde{i}_{qd} = \dfrac{\mathrm{d}\tilde{i}_{qd}}{\mathrm{d}t} = 0 \end{cases} \tag{12}$$

The equivalent continuous input signal is

$$\begin{cases} e_{dq} = K_{odq} \operatorname{sgn}\left(\tilde{i}_{dq}\right) \\ e_{qd} = K_{oqd} \operatorname{sgn}\left(\tilde{i}_{qd}\right) \end{cases} \tag{13}$$

Since $K_{odq} \operatorname{sgn}\left(\tilde{i}_{dq}\right)$, $K_{oqd} \operatorname{sgn}\left(\tilde{i}_{qd}\right)$ are the discontinuous switching value, the filter is needed to get the smooth value.

According to (7), the discretized state equation is

$$\begin{cases} \hat{i}_q(k+1) = G\hat{i}_q(k) + H\left(u(k) - k\,\mathrm{sgn}\left(\hat{i}_q(k) - i_q(k)\right)\right) \\ \hat{i}_q(k+1) = G\hat{i}_q(k) + H\left(u(k) - k\,\mathrm{sgn}\left(\hat{i}_q(k) - i_q(k)\right)\right) \end{cases} \tag{14}$$

where $G = e^{-\frac{R}{L}T}$, $H = \frac{1}{R}\left(1 - e^{-\frac{R}{L}T}\right)$.

## IV. Simulation Analysis

Fig. 6 shows the control block diagram. The stator windings measured by the current sensor and the position signal given by the rotary transformer or linear resistance rule can be transformed to the feedback current by dual *dq* coordinate system. The given values $i_{dd}$ and $i_{qq}$ are equal to zero, the difference of the $i_{dd}$ or $i_{qq}$ and the given values can be used as the input given values of the PI regulator. $i_{dq}$ is the output of PI regulator when the input is the given angular speed and rotary angular speed measured by the resolver encoder. $i_{qd}$ is the output of PI regulator when the input is the given linear velocity and linear position signal measured by the linear resistance rule. $i_{dd}$, $i_{dq}$, $i_{qd}$ and $i_{qq}$ can be derived by dual *dq* transform. Finally, the PWM is generated by space vector modulation to control the motor rotary motion by driving the power switch.

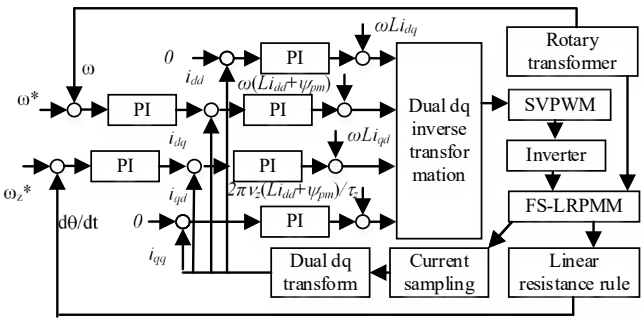


Fig. 6. Control block diagram.

Fig. 7 reveals the PM flux linkage sliding mode observer. The inputs of the model are $i_{dd}$, $i_{qq}$, $i_{dq}$, $i_{qd}$, $U_{qd}$, $U_{dq}$, $\omega$ and $\omega_z$. The output is PM rotary electromotive force of *dq* axis and *qd* axis, which is filtered by a first order low pass filter. Then the output is divided by the motor angular velocity in rotary or linear motion to obtain the observed flux linkage amplitudes.

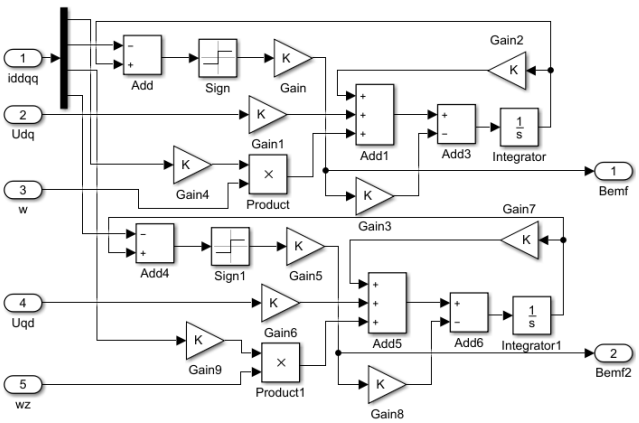


Fig. 7. PM flux linkage sliding mode observer.

The motor start speed is 40 r/min at no load condition, and 3 Nm is added at 0.5 s. Fig. 8 reveals the rotary speed and torque response at start up stage when it works in rotary motion. In the start-up phase, the motor speed and torque have an overshoot of about 37.5% and 66.7%, respectively. The rotary speed and torque can reach the given values in about 0.04 s.

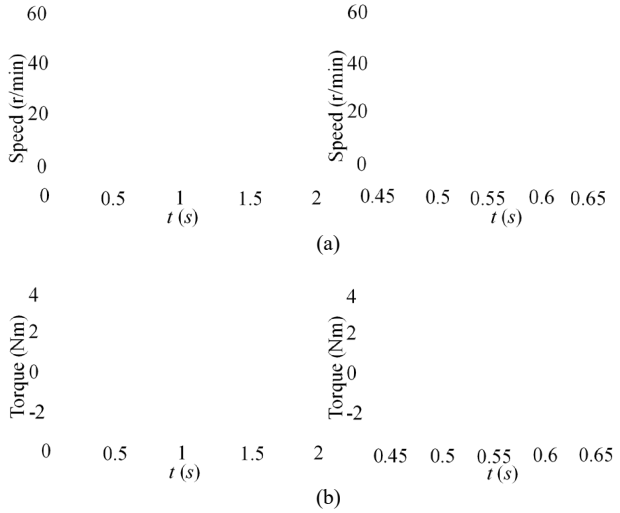


Fig. 8. The rotary speed and torque response at start up stage when it works in rotary motion, (a) rotary speed response, and (b) torque response.

The motor starts at a given linear velocity of 4 mm/s at no load condition, then 30 N is added at 0.5 s. Fig. 9 reveals the linear velocity and thrust response at start up stage when it works in linear motion. When 30 N is added, the linear speed waveform is basically the same, and the response of thrust is not obvious due to high thrust ripple.

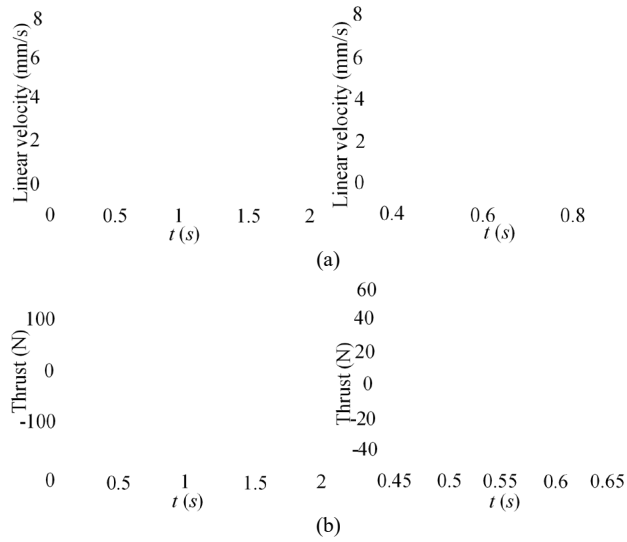


Fig. 9. The linear speed and thrust response at start up stage when it works in linear motion, (a) linear speed response, (b) thrust response.

## V. Experimental Verification

Since there are lots of harmonics in the back EMF waveforms, which is caused by the magnetic flux leakage, the sliding mode variable structure control method is adopted with an improved adaptive flux observer. Both linear and rotary motions are realized through a set of concentrated windings. The key problem is to realize the restraint of detent force and stable operation of linear motion without affecting the torque and thrust characteristics. A sliding mode variable structure control model is established, which is suitable for 2-DOF motion. The primary resistance adaptive law is introduced into

the adaptive observer, which reduces the observation error of the primary flux caused by the change of motor parameters. The experiment is carried out based on cspace motor control experiment platform.

## VI. Conclusions

In order to improve the efficiency of the reelwinder system, a high precision control system of FS-LRM is established using sliding mode control method. The mathematical model is derived by dual-*dq* coordinate system. Since the rotary and linear motions are achieved by only one set of windings, a 2-DOF sliding control observer is built to complete the parameter identification of PM flux linkage, which can reduce the response time of the rotary motion. However, as the amplitude of detent force can generate high thrust ripple, the effect of sliding mode control on the improvement of the linear motion response time is not significant, and there is still a lot of room for improvement.

## References


[1] L. Xie, J. Si, Y. Hu, and H. Feng, "Helical motion analysis of the 2-degree-of-freedom split-stator induction motor," *IEEE Trans. Magn.*, vol. 55, no. 6 , Art. no. 8103705, June 2019.

[2] S. M. Mirić, R. V. Giuffrida, D. Bortis and, J. W. Kolar, "Enhanced complex space vector modeling and control system design of multiphase magnetically levitated rotary–linear machines," *IEEE J. Emerg. Sel. Topics in Power Electron.*, vol. 8, no. 2, pp. 1833-1849, June 2020.

[3] K. Guo, Y. Guo, and J. Li, "Decoupling control analysis of a flux reversal linear rotary permanent magnet actuator," *J. Electr. Eng. Technol.*, vol 15, no.4, pp. 1693–1704, Jul. 2020.

[4] W. Zhao, Z. Chen, D. Xu, J. Ji, and P. Zhao, "Unity power factor fault-tolerant control of linear permanent-magnet vernier motor fed by a floating bridge multilevel inverter with switch fault," *IEEE Trans. Ind. Electron.*, vol. 65, no. 11, pp. 9113-9123, Nov. 2018.

[5] J. Zhao, L. Wang, F. Dong, Z. He, and J. Song, "Robust high bandwidth current regulation for permanent magnet synchronous linear motor drivers by using two-degree-of-freedom controller and thrust ripple observer," *IEEE Trans. Ind. Electron.*, vol. 67, no. 3, pp. 1804-1812, Mar. 2020.

[6] S. Chen, H. Chiang, T. Liu, and C. Chang, "Precision motion control of permanent magnet linear synchronous motors using adaptive fuzzy fractional-order sliding-mode control," *IEEE/ASME Trans. Mechatronics*, vol. 24, no. 2, pp. 741-752, April 2019.

[7] M. A. M. Cheema, J. E. Fletcher, M. F. Rahman, and D. Xiao, "Optimal, combined speed, and direct thrust control of linear permanent magnet synchronous motors," *IEEE Trans. Energy Convers.*, vol. 31, no. 3, pp. 947-958, Sep. 2016.

[8] Y. J. Oh, J. S. Park, B. J. Hyon, and J. Lee, "Novel control strategy of wave energy converter using linear permanent magnet synchronous generator," *IEEE Trans. Appl. Supercond.*, vol. 28, no. 3, pp. 1-5, April 2018, Art no. 5204705.

[9] W. Huang, W. Hua, F. Yin, F. Yu, and J. Qi, "Model predictive thrust force control of a linear flux-switching permanent magnet machine with voltage vectors selection and synthesis," *IEEE Trans. Ind. Electron.*, vol. 66, no. 6, pp. 4956-4967, June 2019.

[10] P. T. Luu, J. Lee, J. Kim, S. Chung, and S. Kwon, "Magnetic sensor design for a permanent magnet linear motor considering edge-effect," *IEEE Trans. Ind. Electron.*, vol. 67, no. 7, pp. 5768-5777, July 2020.

[11] I. Boldea, L. N. Tutelea, W. Xu, and M. Pucci, "Linear electric machines, drives, and MAGLEVs: an overview," *IEEE Trans. Ind. Electron.*, vol. 65, no. 9, pp. 7504-7515, Sept. 2018.

[12] H. Du, X. Chen, G. Wen, X. Yu, and J. Lü, "Discrete-time fast terminal sliding mode control for permanent magnet linear motor," *IEEE Trans. Ind. Electron.*, vol. 65, no. 12, pp. 9916-9927, Dec. 2018.

[13] Z. Pan, F. Dong, J. Zhao, L. Wang, H. Wang, and Y. Feng, "Combined resonant controller and two-degree-of-freedom PID controller for PMSLM current harmonics suppression," *IEEE Trans. Ind. Electron.*, vol. 65, no. 9, pp. 7558-7568, Sept. 2018.

[14] K.Huang, J. Liang, Z. Qian, and J. Li, "An iterative estimation algorithm of prepositioning focusing on the detent force in the permanent magnet linear synchronous motor system," *IEEE Trans. Ind. Electron.*, vol. 67, no. 10, pp. 8252-8261, Oct. 2020.

[15] Li, J. Zhao, Y. Hu, and Z. Wang, "Active disturbance rejection position servo control of PMSLM based on reduced-order extended state observer," *Chinese J. Electr. Eng.*, vol. 6, no. 2, pp. 30-41, June 2020.

[16] Cho, J. Kim, S. B. Choi, and S. Oh, "A high-precision motion control based on a periodic adaptive disturbance observer in a PMLSM," *IEEE/ASME Trans. Mechatronics*, vol. 20, no. 5, pp. 2158-2171, Oct. 2015.

[17] S. Du, J. Hu, Y. Zhu, and M. Zhang, "A Hall sensor-based position measurement with on-line model parameters computation for permanent magnet synchronous linear motor," *IEEE Sensors J.*, vol. 18, no. 13, pp. 5245-5255, July 2018.

[18] L. A. M. Cheema, J. E. Fletcher, D. Xiao, and M. F. Rahman, "A direct thrust control scheme for linear permanent magnet synchronous motor based on online duty ratio control," *IEEE Trans. Power Electron.*, vol. 31, no. 6, pp. 4416-4428, June 2016.

[19] K. Guo, and Y. Guo, "Optimization design of a flux switching linear rotary permanent magnet machine,"*2019 22nd International Conference on Electrical Machines and Systems (ICEMS)*, 2019, pp. 1-6.

[20] K. Guo, "Flux concentrated analysis of flux switching linear rotary permanent magnet machine,"*2020 IEEE International Conference on Applied Superconductivity and Electromagnetic Devices (ASEMD)*, 2020, pp. 1-2.